Aerial Manipulator Pushing a Movable Structure using a DOB-based Robust Controller

Dongjae Lee[1], Hoseong Seo[1], Inkyu Jang[1], Seung Jae Lee[2] and H. Jin Kim[1]

***Abstract*—This paper deals with the problem of an aerial manipulator pushing a movable structure. Contrary to physical interaction with a static structure, suitable consideration of the interacting force during the motion of the structure is required to stably perform this movable structure interaction. To accomplish the task of pushing a structure while ensuring the stability of the aerial manipulator, we present a nonlinear disturbance-observer (DOB)-based robust control approach by regarding the interaction force as a disturbance to the system. Furthermore, to utilize the proposed controller for pushing a movable structure, we propose an algorithm to generate an end-effector position reference that enables safe operation in a realistic situation. We validate the proposed control framework with successful demonstrations on pushing two types of movable structures, a heavy rolling cart (42 [kg]), and a real-like hinged door.**

***Index Terms*—Aerial Systems: Applications, Aerial Systems: Mechanics and Control, Robust/Adaptive Control.**

I. Introduction

AERIAL robots have been extensively studied for over a decade thanks to its inherent strength of high mobility in three-dimensional space. Focused on this strength, aerial robots have been deployed mainly for exploration or surveillance. However, these conventional aerial robots can only perform interaction-free, non-active tasks; therefore, additional ground robots or human operators are required for the physical interaction with the surrounding environment.

To resolve this issue, a new concept of an unmanned aerial manipulator (UAM), which is a platform combining an aerial vehicle and a manipulator, is introduced [1]. Several existing studies [2–9] deal with a situation involving an interaction with a static structure; however, these concepts can be limited due to the unexpected motion of the structure or the time-varying nature of interactions if they were applied to an interaction task of pushing/pulling a *movable structure*: 1) a structure for which pushing/pulling is a more suitable strategy than lifting-and-transporting to move the structure (e.g. a suitcase or a rolling cart); or 2) a structure that is fixed in a certain direction so that only pushing/pulling is available to move the structure (e.g. a drawer or a door). There exist a few papers [10–14] on interaction with a movable structure; nonetheless, none of them explicitly consider the stability in the controller design during the motion of the interacting structure. Therefore, to stably interact with a dynamic structure using a UAM, a new methodology is required.

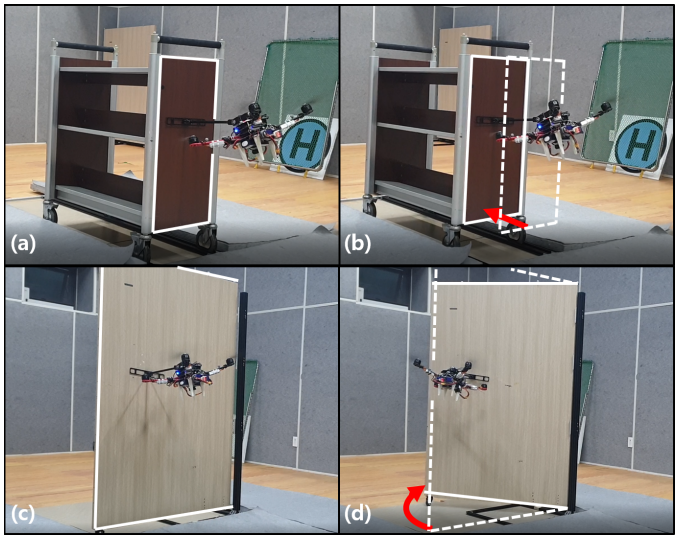

Fig. 1. Experimental results on pushing a rolling cart ((a) and (b)) and a real-like hinged door ((c) and (d)).

A. Related works

1) Movable structure: In [10], experimental results on a conventional, underactuated multirotor-based UAM (mUAM) pushing and pulling a drawer are presented with a dedicated controller for the coupled system dynamics between the mUAM and the drawer. Opening a miniature door is performed in [11] in which a compliant end-effector is designed to grasp a door handle. Nevertheless, both of these papers assume that the interaction force from the motion of the structure is negligible which is not the case for interaction with a structure of a non-negligible inertia. [12] shows an mUAM rotating a valve after perching on it; however, since this task only requires a yawing motion of an mUAM, only one decoupled direction of motion is considered. Finally, in [13], a mechanism design for perching and pushing is proposed for a multirotor to perch and open a hinged door. Although this work shows pushing an actual hinged door, the development of the dedicated platform may require a complex design, and it will be difficult to be employed for other general purpose. Our

Manuscript received: October, 15, 2020; Accepted December, 13, 2020.

This paper was recommended for publication by Editor Pauline Pounds upon evaluation of the Associate Editor and Reviewers' comments. This work was supported by Unmanned Vehicles Core Technology Research and Development Program through the National Research Foundation of Korea (NRF) and Unmanned Vehicle Advanced Research Center (UVARC) funded by the Ministry of Science and ICT, the Republic of Korea (2020M3C1C1A01086411).

[1]Dongjae Lee, Hoseong Seo, Inkyu Jang, and H. Jin Kim are with the Department of Mechanical and Aerospace Engineering, Seoul National University (SNU), and Automation and Systems Research Institute (ASRI), Seoul 08826, South Korea {ehdwo713, hosung37, leplusbon, hjinkim}@snu.ac.kr

[2]Seung Jae Lee is with the Department of Mechanical Engineering, University of California, Berkeley, CA, USA seungjae_lee@berkeley.edu

Digital Object Identifier (DOI): see top of this page.

previous work [14] also performs pushing a real-like hinged door with an mUAM; however, only interaction with a hinged door of known physical properties is considered. Also, position tracking can degrade because the position controller assumes no time delay in both roll and pitch angles.

2) Static structure: As introduced in I-A1, few works on interaction between UAM and a movable structure consider an interacting force due to the motion of the structure in the controller design, which cannot be ignored in general. Given such a lack of previous work, as an alternative, we review state-of-the-art control approaches for the UAM – static-structure interaction.

We categorize existing approaches related with UAM – static-structure interaction control into the following three based on how contact forces are considered[1]: 1) model-based approach [2, 3, 7, 9]; 2) measurement/estimation-based approach [4, 6, 8, 15]; and 3) robust-control-based approach [16, 17]. Most works in the model-based category assume a static environment and model the external force with a quasi-static force. However, this assumption no longer holds when a structure with a non-negligible inertia starts to move with unknown dynamics, and this could lead to tracking performance degradation or even instability.

For the measurement/estimation-based approach, several papers including [4, 6, 8] focus on tracking a force reference and/or tracking an end-effector reference trajectory while maintaining contact with a static surface. Although this force tracking control approach is a possible solution for interaction with a movable structure, further considerations are required for constructing a reference force trajectory to move a structure. Furthermore, most of their algorithms cannot be directly applied to a conventional mUAM since, unlike fully-actuated platforms employed in their works, the full external wrench acting at the end-effector cannot be controlled solely by the multirotor base due to its underactuatedness. The issue from underactuatedness can be overcome by augmenting a multiple-DoF (degrees of freedom) robotic arm to the classical multirotor, and [15] shows a compliant behavior of the mUAM against external force through a rope/bar at the end-effector while [4] executes a constant force tracking with the mUAM in simulations.

In contrast to the two approaches described above where the motion controller directly exploits the knowledge of the external force either from a model or from a measurement/estimation, the robust-control-based approach rather regards the external force as a disturbance to the system and designs a controller robust to such disturbance. As in [16, 17], although only perching on a vertical wall is presented, robust stability can be guaranteed which most of the previous methods do not tackle.

B. Contributions

This paper presents a novel control framework and experimental validation for interaction with different types of movable structures. We propose a two-layered control algorithm: 1) an end-effector position reference generator for the mUAM to make the structure move, and 2) a robust motion controller for tracking the reference while providing robust stability against an interaction force. Particularly, we present a simple yet effective strategy for moving the structure by continuously updating the position reference of the end-effector in the perpendicular direction of the structure's contact surface. In addition, we propose a disturbance-observer-(DOB) based robust position controller which guarantees transient performance recovery [18] of the underactuated subsystem (3) and append the proposed DOB to the DOB structure [19] implemented for the fully-actuated subsystem (2).

In this work, we use $v_i, 0_{j\times k}, \otimes, I_l$, and $\|\cdot\|$ to denote i^{th} component/row of a vector/matrix v, zero matrix in $\mathbb{R}^{j\times k}$, a Kronecker product, an identity matrix in $\mathbb{R}^{l\times l}$, and an induced 2-norm of a matrix. Also, for a column vector a and b, $[a;b] \coloneqq [a^\top\ b^\top]^\top$. Lastly, $c*$ and $s*$ denote shorthands for $\cos(*)$ and $\sin(*)$, respectively.

II. Dynamics

A. Actual dynamics

We consider an mUAM with an n-DoF robotic manipulator. Defining a world frame $\mathscr{F}_W = \{O_W, x_W, y_W, z_W\}$ and a body frame $\mathscr{F}_B = \{O_B, x_B, y_B, z_B\}$ with O_B at the center of mass (CoM) of the mUAM, both using the east-north-up (ENU) convention, we denote the configuration of the mUAM as $q_m = [p_m; \phi; \theta] \in \mathbb{R}^{6+n}$ where $p_m = [p_{m,x}; p_{m,y}; p_{m,z}] \in \mathbb{R}^3$, $\phi = [\phi_x; \phi_y; \phi_z] \in \mathbb{R}^3$, and $\theta = [\theta_1; \cdots; \theta_n] \in \mathbb{R}^n$ are the position, the ZYX Euler angles of the multirotor in $\mathscr{F}_W$, and the joint angles of the robotic manipulator, respectively. The coupled system dynamics of the mUAM can be derived with the Euler-Lagrange equation [19, 20]:

$$M\ddot{q}_m + C\dot{q}_m + G = J\tau_m + \Delta_m \tag{1}$$

where M, C, G are the mass matrix, Coriolis-centrifugal matrix, and gravitational term, $J = \text{blockdiag}\{R_t e_3, Q^\top, I_n\} \in \mathbb{R}^{(6+n)\times(4+n)}$, and $\tau_m = [T; \tau_\phi; \tau_\theta] \in \mathbb{R}^{4+n}$. R_t is the rotation matrix of $\mathscr{F}_B$ with respect to $\mathscr{F}_W$, and Q is the Jacobian matrix satisfying $\omega_B = Q\dot{\phi}$. $\omega_B \in \mathbb{R}^3$ is the angular velocity of $\mathscr{F}_B$ written in $\mathscr{F}_B$, and $e_3 \in \mathbb{R}^3$ is the unit vector in z_W direction. $T \in \mathbb{R}, \tau_\phi \in \mathbb{R}^3, \tau_\theta \in \mathbb{R}^n$ are the multirotor's total thrust in z_B direction, the multirotor's torque in $\mathscr{F}_B$, and joint torques of the robotic manipulator. $\Delta_m \in \mathbb{R}^{6+n}$ is an external disturbance to the system.

As in many other works on mUAM (IV-B in [1]), we deploy an exogenous motion controller for the robotic manipulator and a robust motion controller for the multirotor. For the ease of the following multirotor controller design, we elicit the dynamics of the fully-actuated subsystem $q_f = [p_{m,z}; \phi] \in \mathbb{R}^4$ by pre-multiplying M^{-1} and $E_1 = [0_{4\times2}\ I_4\ 0_{4\times n}] \in \mathbb{R}^{4\times(6+n)}$ sequentially to (1):

$$\ddot{q}_f = F_f + G_f\tau + \Delta_f \tag{2}$$

where $F_f = -E_1M^{-1}(C\dot{q}_m + G)$, $\Delta_f = E_1M^{-1}\Delta_m$, $G_f = E_1M^{-1}JE_2^\top$, $E_2 = [I_4\ 0_{4\times n}]$ and $\tau = [T; \tau_\phi] \in \mathbb{R}^4$ is the control input to the multirotor.

[1]The Approaches that do not directly consider contact forces by employing mechanical compliance as in [5] are neglected in this categorization.

For the underactuated dynamics of the mUAM, which is the horizontal motion in $\mathscr{F}_W$, we construct the dynamics of the CoM of the mUAM as in [19, 21]:

$$\ddot{q}_u = G_u\Phi + \delta_u \tag{3}$$

$$G_u = \frac{T}{m_c}\Psi, \Psi = \begin{bmatrix} c\phi_z & s\phi_z \\ s\phi_z & -c\phi_z \end{bmatrix}, \Phi = \begin{bmatrix} c\phi_x s\phi_y \\ s\phi_x \end{bmatrix},$$

where $q_u = [p_{c,x}; p_{c,y}] \in \mathbb{R}^2$ is the horizontal CoM position of the mUAM in $\mathscr{F}_W$, and m_c is the total mass of the mUAM. δ_u is external disturbance acting in the horizontal direction, including an interacting force. The underactuated subsytem (3) can be controlled by roll and pitch references $\phi_{x,r}, \phi_{y,r}$, and (3) is modified with $\Phi_r = [c\phi_{x,r}s\phi_{y,r}; s\phi_{x,r}] \in \mathbb{R}^2$ as

$$\ddot{q}_u = G_u\Phi_r + \Delta_u \tag{4}$$

where $\Delta_u \coloneqq G_u(\Phi - \Phi_r) + \delta_u$.

B. Nominal dynamics

We first derive the nominal dynamics of the fully-actuated subsystem (2) with the following multirotor dynamics with mass m_c and mass moment of inertia J_B in $\mathscr{F}_B$:

$$\begin{aligned} m_c\ddot{p}_m &= -m_c g e_3 + TR_t e_3 \\ J_B\dot{\omega}_B &= -\hat{\omega}_B J_B\omega_B + \tau_\phi \end{aligned} \tag{5}$$

where $g \in \mathbb{R}$ is the gravitational acceleration constant, and $\hat{*}$ is a hat operator representing the cross product operation as $\hat{a}b = a \times b$. Using $\omega_B = Q\dot{\phi}$ and (5), the nominal dynamics of (2) can be written as

$$\ddot{\bar{q}}_f = \bar{F}_f + \bar{G}_f\bar{\tau} \tag{6}$$

where

$$\bar{F}_f = \begin{bmatrix} -g \\ -Q^{-1}\dot{Q}\dot{\phi} - Q^{-1}J_B^{-1}\hat{\omega}_B J_B\omega_B \end{bmatrix}$$

$$\bar{G}_f = \begin{bmatrix} e_3^\top R_t e_3/m_c & 0_{1\times 3} \\ 0_{3\times 1} & -Q^{-1}\dot{Q}\dot{\phi} - Q^{-1}J_B^{-1}\hat{\omega}_B J_B\omega_B \end{bmatrix},$$

and $\bar{\tau}$ is the nominal control input of τ in the nominal fully-actuated subsystem. Likewise, we define the nominal dynamics of (3) with the nominal control input $\bar{\Phi}_r$ of Φ_r as

$$\ddot{\bar{q}}_u = \bar{G}_u\bar{\Phi}_r \tag{7}$$

where $\bar{G}_u = \bar{T}/m_c\Psi$ with $\bar{T}$ being the nominal value of T.

III. Controller Design

The primary objective in controller design is to guarantee robust performance of the mUAM while interacting with a movable structure. During the interaction, external forces on the system are mainly due to a reaction force from the structure to the mUAM, and this reaction force is highly related to the relative position of the mUAM and the structure. Thus, if the position tracking error of the mUAM is not suitably controlled, the reaction force due to this error could deteriorate the performance and even hinder the stability of the system.

To overcome this issue, we apply a robust motion controller based on nonlinear DOB [18, 19]. Similar to [19], we adopt the DOB design for the fully-actuated subsystem (2), but we further develop and analyze the DOB structure for the underactuated subsystem (4) to ensure transient performance recovery without $\Phi = \Phi_r$ assumption. This transient performance recovery is an essential property for our scenario since the position tracking error of the mUAM can be bounded during both transient and steady-state phases even in the presence of a disturbance.

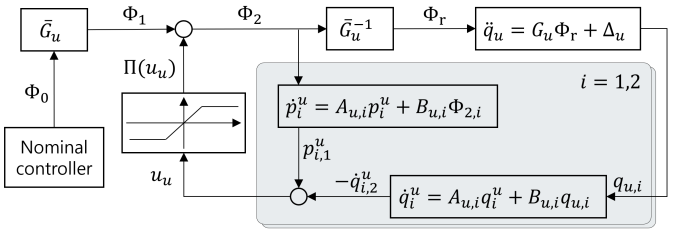

Fig. 2. The proposed inner-loop controller for the underactuated subsystem [18, 19].

A. DOB design for the underactuated subsystem

As in Fig. 2, the inner-loop DOB controller is designed as follows:

$$\begin{aligned} \dot{q}_i^u &= A_{u,i}q_i^u + B_{u,i}q_{u,i}, & \dot{p}_i^u &= A_{u,i}p_i^u + B_{u,i}\Phi_{2,i} \\ u_{u,i} &= p_{i,1}^u - \dot{q}_{i,2}^u, & \Phi_1 &= \bar{G}_u\Phi_0 \\ \Phi_2 &= \bar{G}_u\Phi_0 + \Pi_u(u_u) & \Phi_r &= \Phi_0 + \bar{G}_u^{-1}\Pi_u(u_u) \end{aligned} \tag{8}$$

where $q_i^u = [q_{i,1}^u; q_{i,2}^u] \in \mathbb{R}^2$, $p_i^u = [p_{i,1}^u; p_{i,2}^u] \in \mathbb{R}^2$, and

$$A_{u,i} = \begin{bmatrix} 0 & 1 \\ -a_{i,0}^u/\epsilon_u^2 & -a_{i,1}^u/\epsilon_u \end{bmatrix},\ B_{u,i} = \begin{bmatrix} 0 \\ a_{i,0}^u/\epsilon_u^2 \end{bmatrix}$$

with $a_{i,0}^u$, $a_{i,1}^u$ and ϵ_u being positive parameters to be designed. Also, $q^u = [q_1^u; q_2^u] \in \mathbb{R}^4$, $p^u = [p_1^u; p_2^u] \in \mathbb{R}^4$, and $u_u = [u_{u,1}; u_{u,2}] \in \mathbb{R}^2$. A saturation function $\Pi_u(\cdot)$ is defined as a globally bounded $\mathcal{C}^1$ function satisfying

$$\Pi_u(u) = u\ \forall u \in \mathcal{S}_u,\ \|\partial\Pi_u(u)/\partial u\| \le 1\ \forall u \in \mathbb{R}^2$$
$$\mathcal{S}_u = \left\{u : u = \bar{G}_u G_u^{-1}((\bar{G}_u - G_u)\Phi_0 - \Delta_u)\right\}.$$

Finally, Φ_0 is a control input designed from the nominal dynamics (7).

Assumption 1. *To show transient performance recovery with the proposed inner-loop control law (8), we assume the following:*

1) *External disturbance δ_u, the total thrust T and their time-derivatives $\dot{\delta}_u$, $\dot{T}$ are bounded (but the bounds can be arbitrarily large).*
2) *The solution $[\bar{q}_u(t); \dot{\bar{q}}_u(t); \bar{\Phi}_0(t)]$ of (7), where $\bar{\Phi}_0(t)$ is the outer-loop control law, evolves in an open, connected and bounded set $\mathcal{U} \subset \mathbb{R}^6$ if the initial condition $[\bar{q}_u(0); \dot{\bar{q}}_u(0); \bar{\Phi}_0(0)]$ is located in a known compact set $\mathcal{S} \subset \mathcal{U}$.*

The first assumption on the boundedness of T and $\dot{T}$ is legitimate considering the hardware implementation in which the total thrust T and its time-derivative $\dot{T}$ are bounded mechanically by motor specification. Furthermore, one could

note that the second assumption on the boundedness of the solution $[\bar{q}_u(t); \dot{\bar{q}}_u(t); \bar{\Phi}_0(t)]$ can be easily guaranteed by a simple PD control.

Theorem 1. *Let $\bar{\mathcal{S}}$ be a compact set slightly smaller than $\mathcal{S}$. For a given $\sigma > 0$, there exists ϵ_u^* such that, for each $0 < \epsilon_u \le \epsilon_u^*$, the solution of the actual dynamics (4) and the controller (8) initiated at $[q_u(0); \dot{q}_u(0); \Phi_0(0)] \in \bar{\mathcal{S}}$ and $[p^u(0); q^u(0)] = 0_{8\times1}$ satisfies*

$$|[q_u(t); \dot{q}_u(t); \Phi_0(t)] - [\bar{q}_u(t); \dot{\bar{q}}_u(t); \bar{\Phi}_0(t)]| \le \sigma, \ \ \forall t \ge 0$$

where $[\bar{q}_u(t); \dot{\bar{q}}_u(t); \bar{\Phi}_0(t)]$ is the solution from the nominal dynamics (7) combined with the outer-loop control law Φ_0, with the initial condition $[\bar{q}_u(0); \dot{\bar{q}}_u(0); \bar{\Phi}_0(0)] = [q_u(0); \dot{q}_u(0); \Phi_0(0)]$.

Proof. The proof proceeds in the following three steps as in [18]: 1) transformation of the closed-loop system into a standard singular perturbation form (*Lemma 1*); 2) stability analysis on the fast subsystem (*Lemma 3*) with the help of the derived sector condition (*Lemma 2*); and 3) infinite interval analysis with Tikhonov's theorem [22, 23, p. 434].

As the first step, new coordinates ξ_i and η_i are defined for p_i^u and q_i^u:

$$\begin{aligned}\xi_i &= \begin{bmatrix}\xi_{i,1}\\ \xi_{i,2}\end{bmatrix} = \begin{bmatrix}\frac{1}{\epsilon_u}q_{i,1}^u + \frac{a_{i,1}^u}{a_{i,0}^u}q_{i,2}^u - \frac{1}{\epsilon_u}q_{u,i}\\ q_{i,2}^u - \dot{q}_{u,i}\end{bmatrix} \in \mathbb{R}^2\\ \eta_i &= \begin{bmatrix}\eta_{i,1}\\ \eta_{i,2}\end{bmatrix} = \begin{bmatrix}p_{i,1}^u - \dot{q}_{i,2}^u\\ \epsilon_u(\dot{p}_{i,1}^u - \ddot{q}_{i,2}^u)\end{bmatrix} \in \mathbb{R}^2.\end{aligned} \tag{9}$$

Lemma 1. *With the newly defined coordinates $\xi = [\xi_1; \xi_2] \in \mathbb{R}^4$ and $\eta = [\eta_1; \eta_2] \in \mathbb{R}^4$ in (9), the closed-loop system of the actual dynamics (4) and the inner-loop controller (8) can be transformed into a standard singular perturbation form as*

$$\ddot{q}_u = G_u(\Phi_0 + \bar{G}_u^{-1}\Pi_u(u_u)) + \Delta_u \tag{10a}$$

$$\begin{aligned}\epsilon_u\dot{\xi}_i &= A_{\xi,i}\xi_i - \epsilon_u B_2(G_{u,i}\Phi_r + \Delta_{u,i})\\ \epsilon_u\dot{\eta}_i &= A_{\eta,i}\eta_i + B_2 a_{i,0}^u(\Phi_{2,i} - (G_{u,i}\Phi_r + \Delta_{u,i}))\end{aligned} \tag{10b}$$

where $B_2 = [0; 1]$, and

$$A_{\xi,i} = \begin{bmatrix}-a_{i,1}^u & 1\\ -a_{i,0}^u & 0\end{bmatrix}, \ A_{\eta,i} = \begin{bmatrix}0 & 1\\ -a_{i,0}^u & -a_{i,1}^u\end{bmatrix}.$$

Proof. Please refer to the Appendix A in [24]. ∎

Quasi-steady state of ξ_i and η_i can be obtained from the equation (10b) with $\epsilon_u = 0$:

$$\xi_i^* = \begin{bmatrix}0\\ 0\end{bmatrix}, \ \eta_{i,2}^* = 0, \ \eta_{i,1}^* = \Phi_{2,i} - (G_{u,i}\Phi_r + \Delta_{u,i}) \tag{11}$$

Defining $\eta_{[1]} = [\eta_{1,1}; \eta_{2,1}] \in \mathbb{R}^2$, from the equations (8) and (9), $u_u = \eta_{[1]}$. The quasi-steady state of u_u then can be found from the equations (11) and (8) as

$$\begin{aligned}u_u^* = \eta_{[1]}^* &= \Phi_2 - (G_u\Phi_r + \Delta_u)\\ &= (\bar{G}_u - G_u)\Phi_0 + (I_2 - G_u\bar{G}_u^{-1})\Pi_u(u_u^*) - \Delta_u.\end{aligned} \tag{12}$$

For $u_u \in \mathcal{S}_u$, $\Pi_u(u_u) = u_u$, and the equation (12) can be further arranged as

$$u_u^* = \bar{G}_u G_u^{-1}((\bar{G}_u - G_u)\Phi_0 - \Delta_u). \tag{13}$$

Define a function $\Gamma(\cdot) : \mathbb{R}^2 \to \mathbb{R}^2$ satisfying the following relation which can be obtained by replacing u_u^* with $u_u^* + \delta$ in the equation (12):

$$\begin{aligned}\Gamma(\delta) &= (u_u^* + \delta) - (\bar{G}_u - G_u)\Phi_0\\ &\quad - (I_2 - G_u\bar{G}_u^{-1})\Pi_u(u_u^* + \delta) + \Delta_u\\ &= \delta + (G_u\bar{G}_u^{-1} - I_2)(\Pi_u(u_u^* + \delta) - \Pi_u(u_u^*))\end{aligned} \tag{14}$$

Lemma 2. *By confining the thrust $0 < T < 2\bar{T}$, $\Gamma(\cdot)$ belong to the sector $[1 - \kappa, 1 + \kappa]$ with $0 < \kappa < 1$. Also, $\delta = 0_{2\times1}$ is the unique solution of $\Gamma(\delta) = 0_{2\times1}$.*

Proof. With the equation (14) and the property of the saturation function $\|\partial\Pi_u(u)/\partial u\| \le 1$, the following inequality holds:

$$\begin{aligned}|\Gamma(\delta) - \delta| &\le \left\|G_u\bar{G}_u^{-1} - I_2\right\| \left|\Pi_u(u_u^* + \delta) - \Pi_u(u_u^*)\right|\\ &\le \left\|G_u\bar{G}_u^{-1} - I_2\right\| |\delta|\end{aligned} \tag{15}$$

Substituting $G_u, \bar{G}_u$ into the inequality (15),

$$\kappa := \left\|G_u\bar{G}_u^{-1} - I_2\right\| = \left|\frac{T - \bar{T}}{\bar{T}}\right| < 1.$$

Therefore, by limiting the thrust of the system to meet $0 < T < 2\bar{T}$, $\Gamma(\cdot)$ belongs to the sector $[1 - \kappa, 1 + \kappa]$ with $0 < \kappa < 1$. Also, since $|\Gamma(\delta) - \delta| \le \kappa|\delta|$, $\delta = 0_{2\times1}$ is the unique solution for $\Gamma(\delta) = 0_{2\times1}$. ∎

To analyze the fast dynamics in (10b), error variables are defined as

$$\tilde{\xi} = \xi - \xi^*, \ \tilde{\eta} = \eta - \eta^*, \ \tilde{\eta}_{[1]} = \eta_{[1]} - \eta_{[1]}^*.$$

With the error variables, fast dynamics (10b) is organized with (11) as follows:

$$\begin{aligned}\epsilon_u\dot{\tilde{\xi}} &= A_\xi\tilde{\xi} - \epsilon_u B_2^+(G_u\Phi_0 + G_u\bar{G}_u^{-1}\Pi_u(\eta_{[1]}^* + \tilde{\eta}_{[1]}) + \Delta_u)\\ \epsilon_u\dot{\tilde{\eta}} &= A_{\tilde{\eta}}\tilde{\eta} - B_2^+ a_0^u\Gamma(\tilde{\eta}_{[1]}) - \epsilon_u B_1^+\dot{\eta}_{[1]}^*\end{aligned} \tag{16}$$

where $A_\xi = \text{blockdiag}\{A_{\xi,1}, A_{\xi,2}\}$, $B_i^+ = I_2 \otimes B_i$, $A_{\tilde{\eta}} = \text{blockdiag}\{A_{\tilde{\eta},1}, A_{\tilde{\eta},2}\}$, $a_0^u = \text{diag}\{a_{1,0}^u, a_{2,0}^u\}$, and

$$A_{\tilde{\eta},i} = \begin{bmatrix}0 & 1\\ 0 & -a_{i,1}^u\end{bmatrix}.$$

Remark 1. *The conditions required in Lemma 3 are given in advance by the following remarks.*

1) *The origin of the error dynamics of the fully-actuated subsystem (2) is Lyapunov stable if a stable outer-loop controller for the nominal dynamics (6) is designed with an inner-loop controller in III-B.*
2) *The nominal thrust $\bar{T}$ is taken such that $\bar{T}$ and its time-derivative $\dot{\bar{T}}$ are bounded.*
3) *Given that $q_u, \dot{q}_u$ are bounded, the outer-loop control law Φ_0 is taken such that both Φ_0 and $\dot{\Phi}_0$ are bounded. (e.g. considering the position and yaw references which are bounded and have bounded derivatives, a simple PD control law $\Phi_0 = \bar{G}_u^{-1}(K_p\tilde{q}_u + K_d\dot{\tilde{q}}_u)$ and its derivative $\dot{\Phi}_0$ are bounded due to the two earlier remarks and the fact that the vector field (4) is bounded.)*

Lemma 3. *For $t_f > 0$, there exists $\epsilon_u^* > 0$ such that the solution of (16), initiated from any $\xi(0)$ and $\eta(0)$, satisfies*

$$\left|[\tilde{\xi}(t);\tilde{\eta}(t)]\right| \le \lambda_1 e^{-\lambda_2(t/\epsilon_u)}\left|[\tilde{\xi}(0);\tilde{\eta}(0)]\right| + \Omega(\epsilon_u)$$

for all $t \in [0, t_f]$ and $0 < \epsilon_u \le \epsilon_u^*$, with some positive constants λ_1, λ_2 and a class-$\mathcal{K}$ function Ω.

Proof. We first analyze the stability of the following subsystem of (16):

$$\begin{aligned} \tilde{\eta}' &= A_{\tilde{\eta}}\tilde{\eta} + B_2^+ a_0^u\{-\Gamma(\tilde{\eta}_{[1]})\}, \\ Y &= \Xi\tilde{\eta} = \tilde{\eta}_{[1]}, \Xi = I_2 \otimes [1\ 0] \end{aligned} \tag{17}$$

where $(*)'$ denotes the derivative of $(*)$ with respect to t/ϵ_u. Defining $a_{i,0}, a_{i,1}$ to meet $a_{i,0}/a_{i,1}^2 < 1/2$, the origin of (17) can be proved to be exponentially stable by applying the multivariable circle criterion [23, p. 265] thanks to *Lemma 2*, and there exists a Lyapunov function $V_{\tilde{\eta}} = \tilde{\eta}^\top P_{\tilde{\eta}}\tilde{\eta}$ such that $V_{\tilde{\eta}}' \le -\rho|\tilde{\eta}|^2$ where $P_{\tilde{\eta}} \in \mathbb{R}^{4\times4}$ and $\rho \in \mathbb{R}$ are a positive definite matrix and a positive constant, respectively [25]. Also, since A_ξ is Hurwitz, there exists a positive definite matrix $P_\xi \in \mathbb{R}^4$ such that $P_\xi A_\xi + A_\xi^\top P_\xi = -I_4$.

Now, to derive the inequality in *Lemma 3*, we examine the following Lyapunov candidate function:

$$V_{q_u} = \mu\tilde{\xi}^\top P_\xi\tilde{\xi} + \tilde{\eta}^\top P_{\tilde{\eta}}\tilde{\eta}. \tag{18}$$

Then, the derivative of V_{q_u} with respect to t/ϵ_u follows the following inequality:

$$V_{q_u}' \le -\mu|\tilde{\xi}|^2 - \rho|\tilde{\eta}|^2 + \epsilon_u\mu\nu_1\zeta_1|\tilde{\xi}| + \epsilon_u\nu_2\zeta_2|\tilde{\eta}| \tag{19}$$

where $\nu_1 = 2\left\|P_\xi\right\|$, $\nu_2 = 2\left\|P_{\tilde{\eta}}\right\|$. We set $\zeta_1 = |B_2^+(G_u\Phi_0 + G_u\bar{G}_u^{-1}\Pi_u(\eta_{[1]}^* + \tilde{\eta}_{[1]}) + \Delta_u)|$, $\zeta_2 = |B_1^+\dot{\eta}_{[1]}^*|$ which are all bounded values by *Assumption 1*, *Remark 1* and the saturation function. Then, there always exist positive $\bar{a}_1, \bar{a}_2$ such that the following inequality holds:

$$V_{q_u}' < -\bar{a}_1 V_{q_u} + \epsilon_u\bar{a}_2\sqrt{V_{q_u}}. \tag{20}$$

Finally, employing comparison Lemma [23, pp. 102–103] and quadratic property of the Lyapunov candidate function V_{q_u} to (20), one completes the proof of the *Lemma 3*. ■

Now the exponential stability of the boundary-layer system from *Lemma 3* allows us to obtain the reduced system, which is identical to the nominal dynamics in (7) as follows:

$$\begin{aligned} \ddot{q}_u &= G_u(\Phi_0 + \bar{G}_u\Pi_u(u_u^*)) + \Delta_u \\ &= G_u\Phi_0 + G_u\bar{G}_u^{-1}\Pi_u(u_u^*)) + \Delta_u \\ &= G_u\Phi_0 + ((\bar{G}_u - G_u)\Phi_0 - \Delta_u) + \Delta_u \\ &= \bar{G}_u\Phi_0 \end{aligned} \tag{21}$$

where the outer-loop control law Φ_0 is inserted to the nominal control input $\bar{\Phi}_r$.

Lastly, to show that the reduced system (21) can be obtained in the infinite time interval, we leverage the following two facts. First, there exists t_1 such that the solution $[q_u(t);\dot{q}_u(t);\Phi_0(t)]$ remains in $\mathcal{U}$ for $t \in [0, t_1]$ since the set of initial conditions $\mathcal{S}$ is contained in $\mathcal{U}$ and the vector field (10a) is bounded by the *Assumption 1*, *Remark 1* and the saturation function. On the other hand, there exists $t_2 > 0$ such that $|[q_u(t);\dot{q}_u(t);\Phi_0(t)] - [\bar{q}_u(t);\dot{\bar{q}}_u(t);\bar{\Phi}_0(t)]| \le \sigma/2$ for all $0 \le t \le t_2$, because $[q_u(0);\dot{q}_u(0);\Phi_0(0)] = [\bar{q}_u(0);\dot{\bar{q}}_u(0);\bar{\Phi}_0(0)]$ and, again, the vector field of (10a) is bounded. Finally, let $t_f = \min\{t_1, t_2\}$. Then, *Lemma 3* is applicable, which yields that $|[\xi(t_f);\eta(t_f)]| \to 0$ as $\epsilon_u \to 0$. Since all the assumptions in [22] are satisfied, now Tikhonov's theorem can be applied for the time interval $[t_f, \infty)$ which ends the proof of the theorem. ■

B. DOB design for the fully-actuated subsystem

Similar to that for the underactuated subsystem, the inner-loop controller for the fully-actuated subsystem is designed as follows ($i = 1, 2, 3, 4$):

$$\begin{aligned} \dot{q}_i^f &= A_{f,i}q_i^f + B_{f,i}q_{f,i}, & \dot{p}_i^f &= A_{f,i}p_i^f + B_{f,i}\tau_{2,i} \\ u_{f,i} &= p_{i,1}^f - \Lambda_i(\dot{q}_{i,2}^f - \bar{F}_{f,i}), & \tau_2 &= \Lambda\bar{G}_f\tau_0 + \Pi_f(u_f) \\ \tau &= \tau_0 + (\Lambda\bar{G}_f)^{-1}\Pi_f(u_f) \end{aligned} \tag{22}$$

where $q_i^f = [q_{i,1}^f; q_{i,2}^f] \in \mathbb{R}^2$, $p_i^f = [p_{i,1}^f; p_{i,2}^f] \in \mathbb{R}^2$, and

$$A_{f,i} = \begin{bmatrix} 0 & 1 \\ -a_{i,0}^f/\epsilon_f^2 & -a_{i,1}^f/\epsilon_f \end{bmatrix},\ B_{f,i} = \begin{bmatrix} 0 \\ a_{i,0}^f/\epsilon_f^2 \end{bmatrix}$$

with $a_{i,0}^f$, $a_{i,1}^f$ and ϵ_f are positive parameters to be designed. τ_0 is the outer-loop control input which is designed based on the nominal dynamics (6), and $\Lambda = \mathrm{diag}\{m_c^{(1/2)}, \bar{J}_m^{(1/2)}, \bar{J}_m^{(1/2)}, \bar{J}_m^{(1/2)}\}$ where $\bar{J}_m$ is the minimum value of diagonal terms in J_B. $\Pi_f(\cdot)$ is another saturation function similar to $\Pi_u(\cdot)$.

Following the same proof procedure as in III-A, the transient performance recovery of the actual fully-actuated subsystem (2) to the nominal counterpart (6) can be demonstrated. Detailed proof can be found in [19].

IV. Reference Generation

With the proposed control algorithm (8), (22), it is shown that an mUAM behaves as a nominal multirotor (6), (7) in the presence of a disturbance Δ_u, Δ_f which are bounded and have bounded first derivatives. Therefore, for the case of pushing a movable structure, by assigning a target position of the mUAM beyond the contact surface of the structure, the mUAM is forced to exert more interaction forces to the structure until the mUAM arrives at that target position to which the nominal counterpart converges. This mechanism eventually results in moving the structure; meanwhile, since the transient performance recovery of the mUAM has been verified in *Theorem 1*, the robust stability of the mUAM can be guaranteed during the entire operation.

Based on this concept, we propose an algorithm to generate the end-effector position reference for pushing a movable structure. We relate the mUAM's end-effector position reference $p_{e,r} \in \mathbb{R}^3$ with the velocity of the structure $\dot{p}_s \in \mathbb{R}^3$ such that, for nonzero $\dot{p}_s$, the penetration level of $p_{e,r}$ into the contact surface is inverse proportional to $\dot{p}_s$. Also, if the structure is at rest, we gradually increase $p_{e,r}$, starting from the contact surface of the structure p_s. This increment in the penetration

Algorithm 1 Reference generation algorithm

Input : penetration level δ, update rate Δ_δ
Output : end-effector position reference $p_{e,r}$

if $structure\ at\ rest$ **then**
  $p_s, \phi_s \leftarrow$ getStructurePose();
  $\delta \leftarrow$ forwardUpdate(δ, Δ_δ);
else
  $\delta \leftarrow$ backwardUpdate(δ, Δ_δ);
end
$p_{e,r} \leftarrow$ referenceUpdate(p_s, ϕ_s, δ);
return $p_{e,r}$

level would trigger a faster increase in the interaction force by producing larger values of rolling/pitching motion reference (depending on force exertion direction), while a decrease in the penetration level of $p_{e,r}$ prevents generating an excessively distant reference from the current mUAM's current position. For actual implementation, we realize this idea as in *Algorithm 1*.

If the structure is at rest, the structure's contact surface position p_s is updated, and the penetrating reference $p_{e,r}$ is computed by the increased penetration level δ. On the contrary, if the structure moves, we extract the reference $p_{e,r}$ backward by decreasing δ. This is to restrict a large deviation of the reference from the mUAM's current position. This property is essential in hardware experiments in that it restrains excessive rolling/pitching motion reference (> 50 [deg]) which can cause motor saturation. We acquire the structure's pose (position p_s and orientation $\phi_s \in \mathbb{R}^3$) to adjust to the orientation of the structure, and the structure pose is obtained via an external motion capture system, which can be substituted by an onboard camera.

V. Results

A. Experimental setup

For experimental validation, we build an mUAM with a two-DoF robotic arm composed of a ReadytoSky S500 quadrotor frame, two ROBOTIS Dynamixel XM430 series servomotors, two Turnigy LiPo batteries, and four T-MOTOR ALPHA 40A ESCs, U3 motors, and P12×4 propellers. We harness the OptiTrack motion capture system (MoCap) for localization of the mUAM and movable structures. As the onboard computer, Intel NUC running Robot Operating System (ROS) in Ubuntu 18.04 executes the position control algorithm (i.e. (8) and $i = 1$ case in (22)) and the reference generation algorithm while the customized PX4 firmware of v1.11 in Pixhawk 4 runs attitude control algorithm involving $i = 2, 3, 4$ cases in (22).

We design outer-loop controllers Φ_0 in (8) and τ_0 in (22) as a position PD controller and a cascaded P-PID controller for attitude and angular rate which are sufficient to satisfy *Assumption 1.2*, *Remark 1.3*, and assumptions on an outer-loop controller in [19]. To meet *Remark 1.2*, we set the nominal thrust $\bar{T} = m_c g$ through which the upper bound of the total thrust is defined as $2\bar{T} = 2m_c g$ from *Lemma 2*. Since our application does not require motion in z_W direction, considering only a pitching motion in a hovering condition, a multirotor can reach up to 60 [deg] in the pitch direction, which we believe suffices in our scenarios. Note that a less conservative criterion can be obtained by setting $\bar{T} = T_d$ where T_d is the desired thrust command computed directly from the position controller, but further analysis will be required.

The motors of the robotic arm are each disposed in x_B and y_B directions so that the minimal number of actuators are used to acquire an independent roll and pitch directional orientation of the end-effector from that of the multirotor, motivated by the concept in [26]. With these configurations, to maintain a surface contact with the vertical surface of the structure, the desired angle of each actuator of the robotic arm is set to compensate the multirotor's roll and pitch motion: $\theta_{1,d} = -\phi_x, \theta_{2,d} = -\phi_y$. For yaw directional orientation matching between the end-effector and the structure's contact surface, we set the desired yaw angle to be the yaw angle of the structure's contact surface.

Experiments on each class of *movable structure*, defined in I, are conducted to validate our proposed framework. As a structure belonging to the first class of movable structure, we conduct experiments with a rolling cart, while a real-like hinged door as in [14] is employed for the second class of movable structure. For each type of movable structure, we vary the experimental setting by changing the inertia of the structure in the mUAM's perspective: the former by changing the weight of the structure, and the latter by altering a length of a lever arm. To first validate the performance of the proposed controller in a simpler situation where the structure does not move, we conduct preliminary experiments on interaction with a static structure, but due to the page limit, they are only included in the video attachment.

In Figs. 3 – 6, solid lines and dashed lines are respectively for measurement data and their reference while the dashed line with a triangle marker in the top figure denotes the data of the structure's contact surface. Also, each figure presents the time history of the horizontal position of the end-effector in x_W, y_W direction ($p_{e,x}, p_{e,y}$, top), Euler angles of the mUAM (ϕ_x, ϕ_y, ϕ_z, middle), and joint angles of the robotic arm (θ_1, θ_2, bottom).

B. Pushing a rolling cart

Experimental results on a relatively low inertia (33 [kg]) and high inertia (42 [kg]) can be found in Figs. 1, 3, 4, and 7. In both experiments, as can be found in the top figures of Figs. 3 and 4, the penetrating reference of the robotic arm's end-effector (red, dashed line) goes beyond the position of the structure's contact surface (red, solid line with a triangle marker), driving the mUAM to rotate over 30 [deg] in the pitch direction. In Fig. 3, although the penetrating reference starts to decrease at 4 [s], the pitch angle reference continues to increase until the penetrating reference becomes very small. This suggests that the proposed controller promotes the solution of the actual system to reach the neighborhood of that of the nominal system, by producing a larger pitch angle reference. A similar phenomenon occurs also in Fig. 4 where a slightly higher maximum pitch angle and its reference are obtained. From the bottom figures of Figs. 3, 4, we can

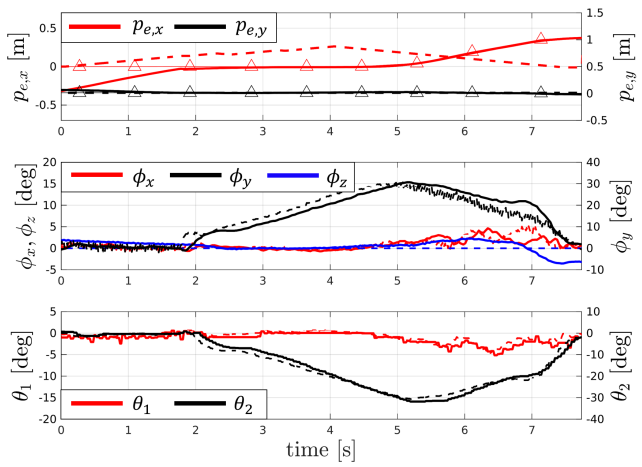

Fig. 3. Pushing a rolling cart with a low inertia (33 [kg]).

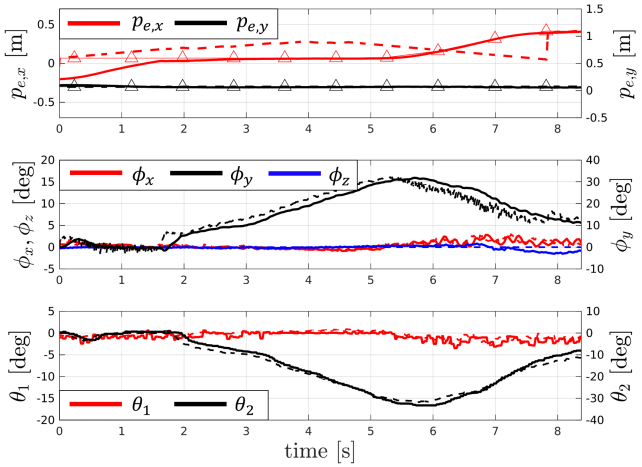

Fig. 4. Pushing a rolling cart with a high inertia (42 [kg]).

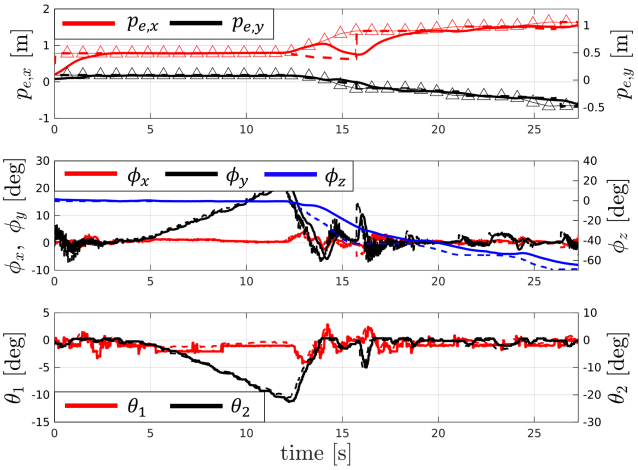

Fig. 5. Pushing a door with a long lever arm length (95 [cm]).

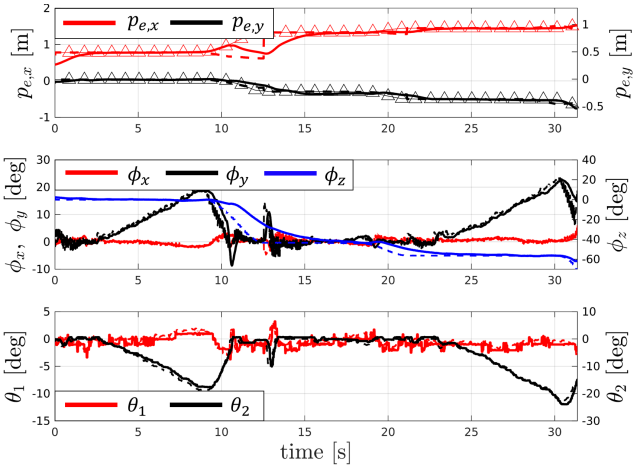

Fig. 6. Pushing a door with a short lever arm length (85 [cm]).

see that the actuators of the robotic arm decently follow the reference angles through which a surface contact between the end-effector and the structure can be secured.

C. Pushing a hinged door

Figs. 1, 5, 6, 8 show experimental results of pushing a hinged door. In contrast to the scenario of pushing a rolling cart, interaction with the hinged door results in additional variation in the contact surface orientation. Therefore, to ensure a steady contact surface orientation matching between the end-effector and the structure, we update the penetration level more conservatively (i.e. smaller) by inserting an if statement between the line number 2 and 3 in *Algorithm 1* for deferring the *forwardUpdate* until the contact surface orientation matching is obtained. As a result, as in Figs. 5 and 6, only little penetrating reference can be found. However, thanks to the proposed controller, although it takes longer time to accumulate the reference pitch angle compared to the results in Figs. 3, 4 (about 2 [s] in Figs. 3, 4 and over 5 [s] in Figs. 5, 6 to reach 20 [deg] from 0 [deg]), the suitable accumulation of the reference pitch angle can still be obtained to move the hinged door. Pushing the hinged door with a shorter moment arm (10 [cm] shorter) in Fig. 6 requires a larger force, and the second pitch reference accumulation from 25 [s] to 30 [s] seems to occur due to this fact and other additional, unintentional friction from the ground.

VI. Conclusion

In this paper, we presented a control framework for an aerial manipulator to push a movable structure. From the controller in [19], by augmenting the nonlinear DOB also to the underactuated subsystem, we could guarantee the transient performance recovery of both the underactuated subsytem and the fully-actuated subsystem which constitute the overall mUAM system, given an exogenous joint controller of the robotic arm. Next, we introduced the algorithm to generate the end-effector position reference for pushing a movable structure. Validation of the proposed framework was accomplished by experiments with a rolling cart and a real-like hinged door. During the interaction, over 30 [deg] of pitching motion is produced to push the rolling cart while safe operation can be maintained even during an interaction with a moving structure. For future work, we expect to expand the proposed framework to handle an interaction with an arbitrary structure movable in any direction in 2-dimensional space.

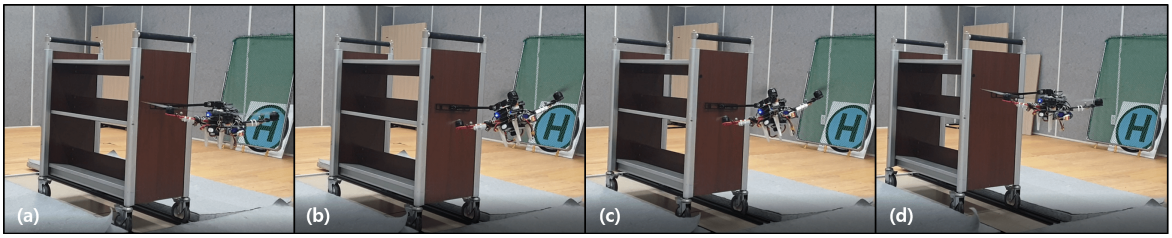

Fig. 7. A customized mUAM pushing a rolling cart. Alphabetic order from (a) to (d) indicates the time sequence whose total elapsed time is about 10 seconds.

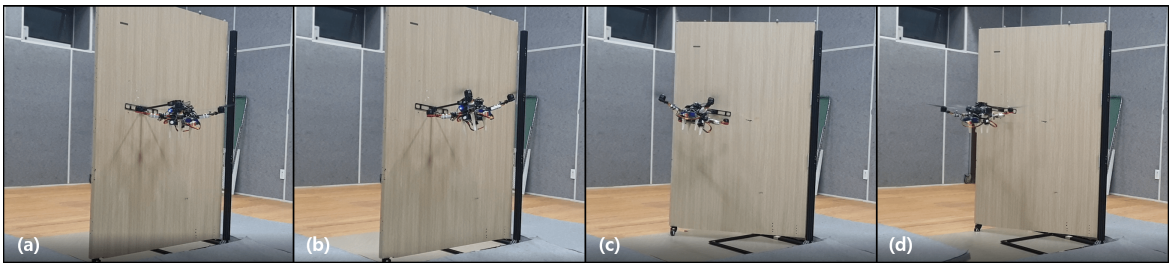

Fig. 8. A customized mUAM pushing a real-like hinged door. Alphabetic order from (a) to (d) indicates the time sequence whose total elapsed time is about 30 seconds.

REFERENCES

[1] F. Ruggiero, V. Lippiello, and A. Ollero, "Aerial manipulation: A literature review," *IEEE Robotics and Automation Letters*, vol. 3, no. 3, pp. 1957–1964, 2018.

[2] S. Hamaza, I. Georgilas, M. Fernandez, P. Sanchez, T. Richardson, G. Heredia, and A. Ollero, "Sensor installation and retrieval operations using an unmanned aerial manipulator," *IEEE Robotics and Automation Letters*, vol. 4, no. 3, pp. 2793–2800, 2019.

[3] D. Tzoumanikas, F. Graule, Q. Yan, D. Shah, M. Popovic, and S. Leutenegger, "Aerial manipulation using hybrid force and position nmpc applied to aerial writing," *arXiv preprint arXiv:2006.02116*, 2020.

[4] G. Nava, Q. Sablé, M. Tognon, D. Pucci, and A. Franchi, "Direct force feedback control and online multi-task optimization for aerial manipulators," *IEEE Robotics and Automation Letters*, vol. 5, no. 2, pp. 331–338, 2019.

[5] M. Tognon, H. A. T. Chávez, E. Gasparin, Q. Sablé, D. Bicego, A. Mallet, M. Lany, G. Santi, B. Revaz, J. Cortés, *et al.*, "A truly-redundant aerial manipulator system with application to push-and-slide inspection in industrial plants," *IEEE Robotics and Automation Letters*, vol. 4, no. 2, pp. 1846–1851, 2019.

[6] K. Bodie, M. Brunner, M. Pantic, S. Walser, P. Pfändler, U. Angst, R. Siegwart, and J. Nieto, "An omnidirectional aerial manipulation platform for contact-based inspection," *Robotics: Science and System XV*, vol. 15, 2019.

[7] H. W. Wopereis, W. L. Van De Ridder, T. J. Lankhorst, L. Klooster, E. M. Bukai, D. Wuthier, G. Nikolakopoulos, S. Stramigioli, J. B. Engelen, and M. Fumagalli, "Multimodal aerial locomotion: An approach to active tool handling," *IEEE Robotics & Automation Magazine*, vol. 25, no. 4, pp. 57–65, 2018.

[8] M. Ryll, G. Muscio, F. Pierri, E. Cataldi, G. Antonelli, F. Caccavale, D. Bicego, and A. Franchi, "6d interaction control with aerial robots: The flying end-effector paradigm," *The International Journal of Robotics Research*, vol. 38, no. 9, pp. 1045–1062, 2019.

[9] X. Meng, Y. He, and J. Han, "Hybrid force/motion control and implementation of an aerial manipulator towards sustained contact operations," in *2019 IEEE/RSJ International Conference on Intelligent Robots and Systems (IROS)*. IEEE, 2019, pp. 3678–3683.

[10] S. Kim, H. Seo, and H. J. Kim, "Operating an unknown drawer using an aerial manipulator," in *2015 IEEE International Conference on Robotics and Automation (ICRA)*. IEEE, 2015, pp. 5503–5508.

[11] D. R. McArthur, A. B. Chowdhury, and D. J. Cappelleri, "Autonomous door opening with the interacting-boomcopter unmanned aerial vehicle," *Journal of Mechanisms and Robotics*, vol. 12, no. 2, 2020.

[12] M. Orsag, C. Korpela, S. Bogdan, and P. Oh, "Dexterous aerial robots—mobile manipulation using unmanned aerial systems," *IEEE Transactions on Robotics*, vol. 33, no. 6, pp. 1453–1466, 2017.

[13] H. Tsukagoshi, M. Watanabe, T. Hamada, D. Ashlih, and R. Iizuka, "Aerial manipulator with perching and door-opening capability," in *2015 IEEE International Conference on Robotics and Automation (ICRA)*. IEEE, 2015, pp. 4663–4668.

[14] D. Lee, H. Seo, D. Kim, and H. J. Kim, "Aerial manipulation using model predictive control for opening a hinged door," in *2020 IEEE International Conference on Robotics and Automation (ICRA)*, 2020, pp. 1237–1242.

[15] E. Cataldi, G. Muscio, M. A. Trujillo, Y. Rodríguez, F. Pierri, G. Antonelli, F. Caccavale, A. Viguria, S. Chiaverini, and A. Ollero, "Impedance control of an aerial-manipulator: Preliminary results," in *2016 IEEE/RSJ International Conference on Intelligent Robots and Systems (IROS)*. IEEE, 2016, pp. 3848–3853.

[16] F. Forte, R. Naldi, A. Macchelli, and L. Marconi, "On the control of an aerial manipulator interacting with the environment," in *2014 IEEE International Conference on Robotics and Automation (ICRA)*. IEEE, 2014, pp. 4487–4492.

[17] R. Naldi, A. Macchelli, N. Mimmo, and L. Marconi, "Robust control of an aerial manipulator interacting with the environment," *IFAC-PapersOnLine*, vol. 51, no. 13, pp. 537–542, 2018.

[18] J. Back and H. Shim, "An inner-loop controller guaranteeing robust transient performance for uncertain mimo nonlinear systems," *IEEE Transactions on Automatic Control*, vol. 54, no. 7, pp. 1601–1607, 2009.

[19] S. Kim, S. Choi, H. Kim, J. Shin, H. Shim, and H. J. Kim, "Robust control of an equipment-added multirotor using disturbance observer," *IEEE Transactions on Control Systems Technology*, vol. 26, no. 4, pp. 1524–1531, 2017.

[20] S. Kim, S. Choi, and H. J. Kim, "Aerial manipulation using a quadrotor with a two dof robotic arm," in *2013 IEEE/RSJ International Conference on Intelligent Robots and Systems*. IEEE, 2013, pp. 4990–4995.

[21] H. Yang and D. Lee, "Dynamics and control of quadrotor with robotic manipulator," in *2014 IEEE international conference on robotics and automation (ICRA)*. IEEE, 2014, pp. 5544–5549.

[22] F. C. Hoppensteadt, "Singular perturbations on the infinite interval," *Transactions of the American Mathematical Society*, vol. 123, no. 2, pp. 521–535, 1966.

[23] H. K. Khalil and J. W. Grizzle, *Nonlinear systems*. Prentice hall Upper Saddle River, NJ, 2002, vol. 3.

[24] J. S. Bang, H. Shim, S. K. Park, and J. H. Seo, "Robust tracking and vibration suppression for a two-inertia system by combining backstepping approach with disturbance observer," *IEEE Transactions on Industrial Electronics*, vol. 57, no. 9, pp. 3197–3206, 2009.

[25] J. Back and H. Shim, "Adding robustness to nominal output-feedback controllers for uncertain nonlinear systems: A nonlinear version of disturbance observer," *Automatica*, vol. 44, no. 10, pp. 2528–2537, 2008.

[26] S. J. Lee, D. Lee, J. Kim, D. Kim, I. Jang, and H. J. Kim, "Fully-actuated autonomous flight of thruster-tilting multirotor," *IEEE/ASME Transactions on Mechatronics*, 2020.